Huchon, P., Taylor, B., and Klaus, A. (Eds.)
Proceedings of the Ocean Drilling Program, Scientific Results Volume 180

20. Data Report: Rock Magnetic Parameters of the Topmost Sediments of ODP Sites 1109, 1110, and 1115 in the Woodlark Basin[1]

Naoto Ishikawa[2] and Gina Marie Frost[3]

ABSTRACT

Rock magnetic measurements were performed on sediments above 20 meters below seafloor (mbsf) (general) and above 2.5 mbsf (detailed) at Sites 1109, 1110, and 1115 (Ocean Drilling Program Leg 180) in the western Woodlark Basin. Rock magnetic parameters imply the presence of magnetite as a principal magnetic mineral in the sediments. The hysteresis ratios lay in the pseudo–single domain field and generally showed the trend close to that for the mixture of single domain and multidomain magnetite The sediments in the oxidized zones at the top at Sites 1109 and 1115 provided a different trend in the logarithmic plot of the hysteresis ratios, and the oxidized samples were characterized by higher coercivity.

INTRODUCTION

Magnetic information in sediments derived by paleomagnetic and rock magnetic methods has been used for a better understanding of the Earth system. Sediments change their magnetic properties through diagenetic changes and authigenic formation of magnetic minerals after deposition. As a result, some parts of the magnetic information are probably lost or some are possibly emphasized. It is thus important to clarify the process of magnetic change for evaluating the magnetic in-

[1]Ishikawa, N., and Frost, G.M., 2002. Data report: Rock magnetic parameters of the topmost sediments of ODP Sites 1109, 1110, and 1115 in the Woodlark Basin. *In* Huchon, P., Taylor, B., and Klaus, A. (Eds.), *Proc. ODP, Sci. Results,* 180, 1–15 [Online]. Available from World Wide Web: <http://www-odp.tamu.edu/publications/180_SR/VOLUME/CHAPTERS/162.PDF>. [Cited YYYY-MM-DD]
[2]Graduate School of Human and Environmental Studies, Kyoto University, Sakyo-ku, Kyoto 606-8501, Japan.
ishikawa@gaia.h.kyoto-u.ac.jp
[3]Central Oregon Community College, 2600 Northwest College Way, Bend OR 97701-5998, USA.

Initial receipt: 24 December 2000
Acceptance: 25 September 2001
Web publication: 15 February 2002
Ms 180SR-162

formation in sediments, which also reveals information regarding the sedimentary environment.

In order to analyze changes of magnetic properties at the top of sediment cores, samples were taken from advanced piston cores (APCs) from Sites 1109, 1115, and 1110 (Ocean Drilling Program Leg 180) in the western Woodlark Basin. Sediments were sampled above ~20 meters below seafloor (mbsf), with short-interval sampling above ~2.5 mbsf. Rock magnetic data of the sediments are reported in this paper.

SAMPLES

Site 1109 is located 11 km north of the Moresby Seamount (Fig. F1), and APC coring occurred in three holes. Samples in this study were taken from Cores 180-1109A-1H and 180-1109C-2H and 3H at Site 1109. The cores consist of Pleistocene hemipelagic calcareous clay and silt accumulated at middle bathyal depths (Shipboard Scientific Party, 1999a). Nannofossil oozes rich in clay are present above 6 meters below seafloor (mbsf). These sediments range in color from brown in the uppermost 14.5-cm-thick oxidized interval to greenish gray below this position. Coarse- and fine-grained sand with foraminifers was recognized between 3.0 and 3.5 and between 8.4 and 9.5 mbsf, respectively.

Site 1115 is located ~30 km north of Site 1109 (Fig. F1). APC coring occurred in Holes 1115A and 1115B. Samples were obtained from Cores 180-1115A-1H and 180-1115B-1H to 3H. The cores consist of nannofossil ooze, which range in color from yellowish brown in the top 20 cm to greenish gray below this position (Shipboard Scientific Party, 1999b). These sediments accumulated at upper middle bathyal depths.

Site 1110 is located near the foot of Moresby Seamount (Fig. F1). From Hole 1110A, 9.5 m of fine-grained Pleistocene sediments that accumulated in deep water were recovered; the sediments were characterized by the abundance of turbidites (Shipboard Scientific Party, 1999c). Core 180-1110A-1H consists of 7 m of mainly nannofossil-rich foraminifer ooze and silty clay, which ranges in color from olive to gray. Silt between 6 and 7 mbsf was volcaniclastic with >70% colorless glass shards.

Samples that contained ~5 cm^3 of sediment were obtained at 10-cm intervals above 2.5 mbsf by pushing two plastic tubes, each about 1 cm in diameter, into the working half of core sections. Below 2.5 mbsf, one sample was obtained from each core section down to 6.3 mbsf for Hole 1110A, to 20.5 mbsf for Holes 1109A and 1109C, and to 20.6 mbsf for Holes 1115A and 1115B. Volcanic ash layers were not sampled. Each sample was sealed in a plastic bag, which was kept cold on board ship and during transportation to and in the laboratory.

METHODS

Rock magnetic parameters were obtained using an alternating gradient–force magnetometer (Princeton Measurement Corporation, Micro-Mag Model 2900-02) at Kyoto University. Wet small chips of 10–30 mg were prepared for rock magnetic analysis. Each chip was lapped by an ~8-mm^2 piece of aluminum foil (~3 mg). For estimating the magnetic effect of the aluminum foil, hysteresis loop measurements were performed repeatedly on a nickel standard sample and the same sample lapped by a piece of the aluminum foil (~3 mg). The hysteresis measurement on the aluminum foil was unsuccessful because of the failure in

F1. Map showing localities of ODP Sites 1109, 1115, and 1110, p. 7.

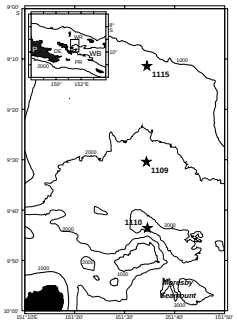

optimization according to the ordinary MicroMag procedure. The result of the hysteresis measurements for the nickel standard sample is listed in Table T1. The difference in the coercivity (H_c), saturation magnetization (M_s), saturation remanent magnetization (M_r), and M_r/M_s was not significant. The value of high-field slope between 0.7 and 1.0 T was different between the standard sample and the sample lapped by the aluminum foil. The ~3 mg of aluminium foil was found to provide a paramagnetic effect of ~32 nAm^2/T, although pure aluminum is diamagnetic.

Each chip was subjected to two kind of measurements: a hysteresis loop (HL) measurement using a maximum field of 1.0 T and direct-current demagnetization (DCD) of a saturation isothermal remanent magnetization (SIRM) imparted at 1.0 T. For each HL, the coercivity (H_c), saturation magnetization (M_s), and saturation remanent magnetization (M_r) were determined after correction for the high-field slope between 0.7 and 1.0 T. Field increments were 10 mT in high field between 0.5 (–0.5) and 1.0 (–1.0) T, 5 mT between 0.1 (–0.1) and 0.5 (–0.5) T, and 2 mT between 0.1 and –0.1 T. Two types of DCD measurements were performed. A DCD was measured at 2-mT increments below 100 mT to determine the coercivity of remanence (H_{cr}). A DCD was also measured at 0.1-T increments up to 0.3 T, which provided values of SIRM, isothermal remanent magnetization (IRM) backfield at 0.1 T, and IRM backfield at 0.3 T. S-ratios (S[–0.1 T] and S[–0.3 T]) were calculated after King and Channell (1991) as follows:

$$S(-0.1\ \mathrm{T}) = -[\mathrm{IRM}(-0.1\ \mathrm{T})/\mathrm{SIRM}] \text{ and}$$

$$S(-0.3\ \mathrm{T}) = -[\mathrm{IRM}(-0.3\ \mathrm{T})/\mathrm{SIRM}].$$

RESULTS AND DISCUSSION

Rock magnetic parameters are listed in Table T2 and plotted in Figures F2, F3, F4, and F5. Magnetic susceptibility data measured on the multisensor track on board ship are also shown. The examples of hysteresis loops are shown in Figure F6. Magnetic features above 2.5 mbsf are described in detail in the following section.

Site 1109

M_r and M_s values increased gradually from the surface down to 1.6 mbsf, followed by decreasing values downward to 2.3 mbsf (Fig. F2). The change in the values was approximately consistent with magnetic susceptibility variation. The consistency seemed to be observed in the samples below 3.5 mbsf although it was less clear because of the larger sampling interval. The S(–0.3 T) values were >0.85, especially ~0.95 in the section above 2.3 mbsf. It may be implied that ferrimagnetic magnetite is a principal magnetic mineral and that the contribution of high-coercivity minerals (hematite and goethite) is low. The magnetic susceptibility values possibly reflect the concentration of magnetite.

In the section above 2.3 mbsf, the three samples of the brown-colored sediments from the oxidized zone at the top provided remarkable magnetic features; the three samples had small S(–0.1 T) values of 0.6 and high H_{cr} of ~42 mT. The samples also showed slightly higher H_c values. Below this position, the S(–0.1 T) values were ~0.8 and the H_c and

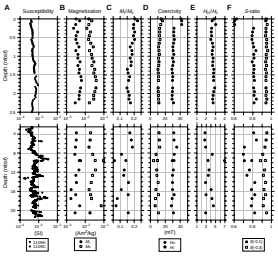

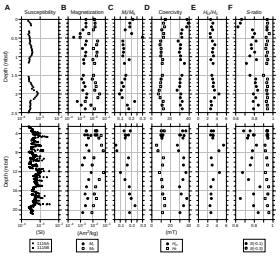

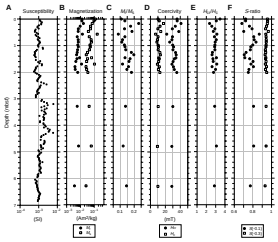

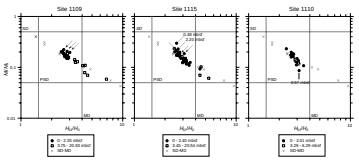

H_{cr} values were ~10 and 30 mT, respectively. Hysteresis loops of the sample from the oxidized zone and that below the zone are shown in Figure F6A and F6B, respectively. The M_r/M_s below the oxidized zone decreased down to 1.6 mbsf and then increased downward to 2.3 mbsf. The change of the H_{cr}/H_c was contrary to that of the M_r/M_s. The variation in the M_r/M_s and H_{cr}/H_c may reflect the change in the average grain size of magnetite. In the logarithmic plot of M_r/M_s against H_{cr}/H_c (Parry et al., 1982) (Fig. F5), data for the samples plotted in the pseudo–single domain (PSD) region of the Day et al (1977) plot. All data except the three samples at the top fit a tight girdle, which is close to the trend for the mixture of single domain (SD) and mulitidomain (MD) magnetite of Parry (1982). The three samples at the top followed a different trend. The lower S(–0.1 T) and higher H_{cr} of the three samples may imply the presence of high-coercivity magnetic minerals such as hematite and goethite and their larger contribution to magnetic signal in the oxidized zone, although there was no difference in the S(–0.3 T) value between the oxidized samples and the others.

Site 1115

M_r and M_s values showed notable decreases at 0.4–0.5 and 2.2 mbsf, where no remarkable change was observed in magnetic susceptibility data (Fig. F3). The hysteresis loop of the samples with low M_r and M_s values showed low contribution of ferromagnetic signal (Fig. F6D). Except for the positions, the general trend of the change in the M_r and M_s values seemed consistent with that of magnetic susceptibility variation (Fig. F3). The S(–0.3 T) values were >0.9 throughout all samples, implying the presence of magnetite as a principal ferrimagnetic mineral. Magnetic susceptibility is possibly controlled by the concentration of magnetite. The M_r and M_s values inferred the low concentration of magnetite at 0.4–0.5 and 2.2 mbsf, which was not indicated from susceptibility data. This difference might have been attributed to the heterogeneity in the sample at those positions.

The lower values (0.6–0.7) of S(–0.1 T) were recognized in the three samples from the oxidized sediments (yellowish brown color) at the top. The three samples also showed relatively higher values of the H_{cr} and H_c. This magnetic feature is similar to that of the oxidized samples at the top of Site 1109. The hysteresis loops of the samples in the oxidized zone at Sites 1115 and 1109 also seem to be similar (Fig. F6). In the logarithmic plot of the M_r/M_s against H_{cr}/H_c, the data generally plotted in the PSD region. Except for the samples in the oxidized zone and those with low M_r and M_s values at 0.4–0.5 and 2.2 mbsf, the data seems to lie on a linear trend. The trend is approximately close to the trend for the mixture of SD and MD magnetite of Parry (1982).

Site 1110

The change in the M_r and M_s values was approximated that in magnetic susceptibility data above ~1 mbsf, whereas below ~1 mbsf the relationship was obscure (Fig. F4). The S(–0.3 T) values of ~0.95 were consistent throughout the samples, which probably indicates the presence of magnetite as a principal ferrimagnetic mineral.

The S(–0.1 T) value ranged between 0.68 and 0.87, and the value was larger at ~70 and ~170 mbsf and smaller around the top and at ~140 mbsf. The H_{cr} and H_c values showed an opposing trend, although the

F6. Examples of hysteresis loops before and after slope correction, p. 12.

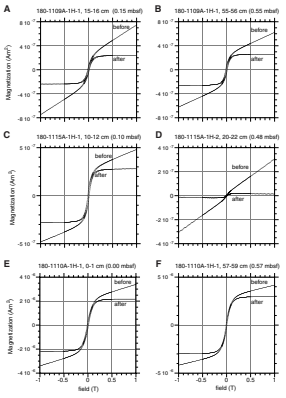

variation in the H_c value was less remarkable. These features possibly imply the change in average grain size of magnetite. Many structures with normal grading produced by turbidites were recognized in the APC cores of Site 1110 (Shipboard Scientific Party, 1999c). The grain size change of magnetite inferred by rock magnetic parameters might have been influenced by turbidity current. In the log-log plot of hysteresis ratios (Parry, 1982), the data fitted a girdle in the PSD region and lay approximately on the trend for the mixture of SD and MD magnetite of Parry (1982). The sample at 0.57 mbsf, however, appeared to have hysteresis ratios different from the trend of the other samples. This sample had larger M_r and M_s values and was characterized by low coercivity (higher S[–0.1 T] and lower H_{cr} and H_c). The hysteresis loop of this sample is shown in Figure **F6E.** The samples at the top of Site 1110 did not show the remarkable magnetic features observed in the samples from the oxidized zone at Sites 1109 and 1115. The color of the sediments implies less oxidation at the top of Site 1110.

ACKNOWLEDGMENTS

We appreciate the critical reviewing of Dr. C.E. Geiss. We thank all other participants of Leg 180 Shipboard Scientific Party, technicians, and crew of the *JOIDES Resolution*.

This research used samples and/or data provided by the Ocean Drilling Program (ODP). ODP is sponsored by the U.S. National Science Foundation (NSF) and participating countries under management of Joint Oceanographic Institutions (JOI), Inc.

REFERENCES

Day, R., Fuller, M., and Schmidt, V.A., 1977. Hysteresis properties of titanomagnetites: grain-size and compositional dependence. *Phys. Earth Planet. Inter.,* 13:260–267.

King, J.W., and Channell, J.E.T., 1991. Sedimentary magnetism, environmental magnetism, and magentostratigraphy. *Rev. Geophys., Suppl.,* 29:358–370.

Parry, L.G., 1982. Magnetization of immobilized particle dispersions with two distinct particle sizes. *Phys. Earth Planet. Inter.,* 28:230–241.

Shipboard Scientific Party, 1999a. Site 1109. *In* Taylor, B., Huchon, P., Klaus, A., et al., *Proc. ODP, Init. Repts.,* 180, 1–298 [CD-ROM]. Available from: Ocean Drilling Program, Texas A&M University, College Station, TX 77845-9547, U.S.A.

————, 1999b. Site 1115. *In* Taylor, B., Huchon, P., Klaus, A., et al., *Proc. ODP, Init. Repts.,* 180, 1–226 [CD-ROM]. Available from: Ocean Drilling Program, Texas A&M University, College Station, TX 77845-9547, U.S.A.

————, 1999c. Sites 1110–1113. *In* Taylor, B., Huchon, P., Klaus, A., et al., *Proc. ODP, Init. Repts.,* 180, 1–89 [CD-ROM]. Available from: Ocean Drilling Program, Texas A&M University, College Station, TX 77845-9547, U.S.A.

Taylor, B., Huchon, P., Klaus, A., et al., 1999. *Proc. ODP, Init. Repts.,* 180 [CD-ROM], Available from: Ocean Drilling Program, Texas A&M University, College Station, TX 77845-9547, U.S.A.

Figure F1. Map showing localities of ODP Sites 1109, 1115, and 1110 (Leg 180) in the western Woodlark Basin (WB). P = Papuan Peninsula, DE = D'Entrecasteaux Island, WR = Woodlark Rise, PR = Pocklington Rise (modified from Taylor, Huchon, Klaus, et al., 1999).

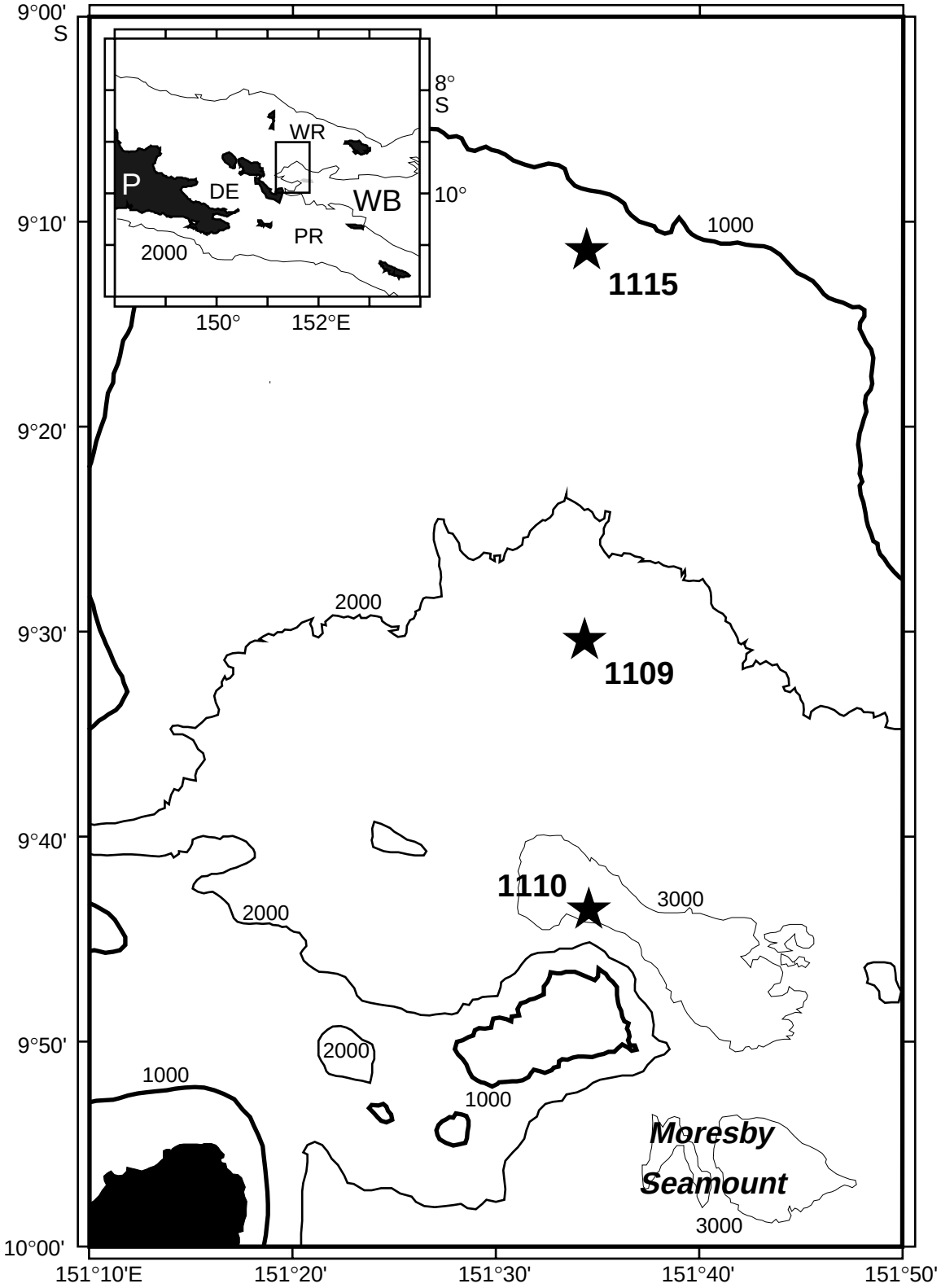

Figure F2. Depth variation of rock magnetic parameters at Site 1109. **A.** Shipboard volume magnetic susceptibility (Taylor, B., Huchon, P., Klaus, A., et al., 1999). **B.** Saturation remanent magnetization (M_r) and saturation magnetization (M_s). **C.** Ratio of M_r to M_s. **D.** Coercivity (H_c) and coercivity of remanence (H_{cr}). **E.** Ratio of H_{cr} to H_c. **F.** Ratios of isothermal remanence at backfields of 0.1 T (S[–0.1 T]) and 0.3 T (S[–0.3 T]) to M_r, respectively.

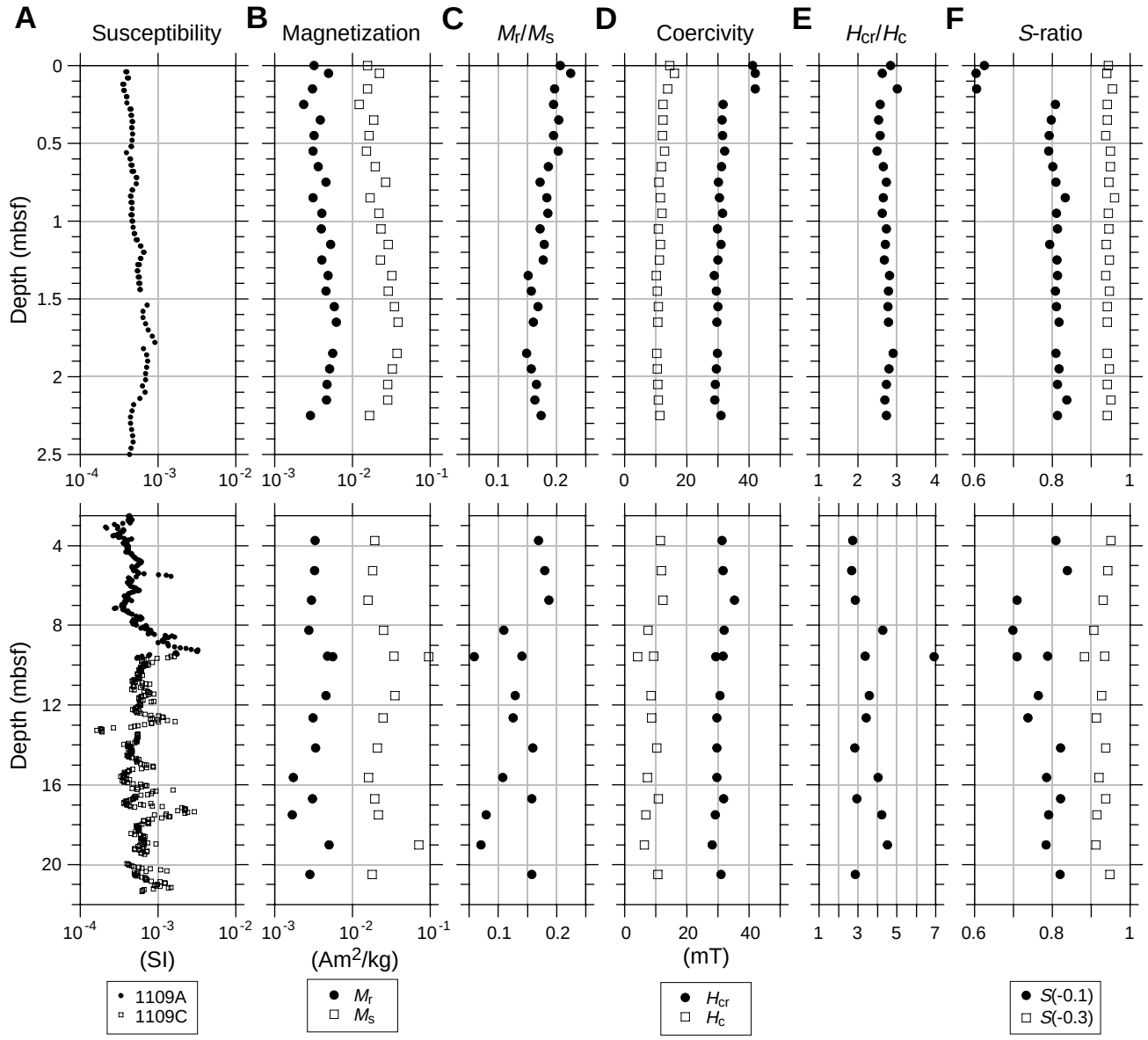

Figure F3. Depth variation of rock magnetic parameters at Site 1115. **A.** Shipboard volume magnetic susceptibility (Taylor, Huchon, Klaus, et al., 1999). **B.** Saturation remanent magnetization (M_r) and saturation magnetization (M_s). **C.** Ratio of M_r to M_s. **D.** Coercivity (H_c) and coercivity of remanence (H_{cr}). **E.** Ratio of H_{cr} to H_c. **F.** Ratios of isothermal remanence at backfields of 0.1 T (S[–0.1 T]) and 0.3 T (S[–0.3 T]) to M_r, respectively.

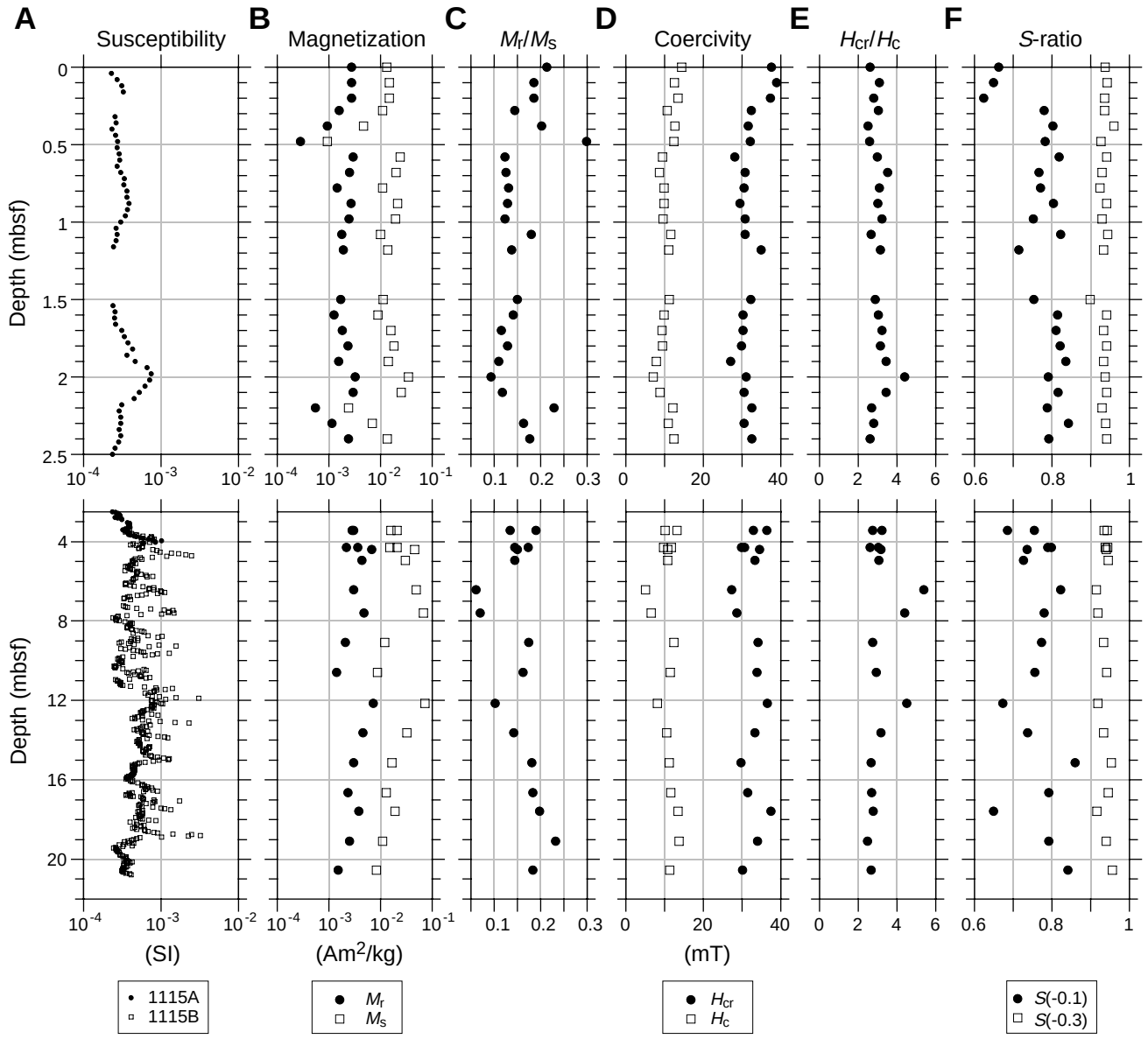

Figure F4. Depth variation of rock magnetic parameters at Site 1110. **A.** Shipboard volume magnetic susceptibility (Taylor, B., Huchon, P., Klaus, A., et al., 1999). **B.** Saturation remanent magnetization (M_r) and saturation magnetization (M_s). **C.** Ratio of M_r to M_s. **D.** Coercivity (H_c) and coercivity of remanence (H_{cr}). **E.** Ratio of H_{cr} to H_c. **F.** Ratios of isothermal remanence at backfields of 0.1 T (S[–0.1 T]) and 0.3 T (S[–0.3 T]) to M_r, respectively.

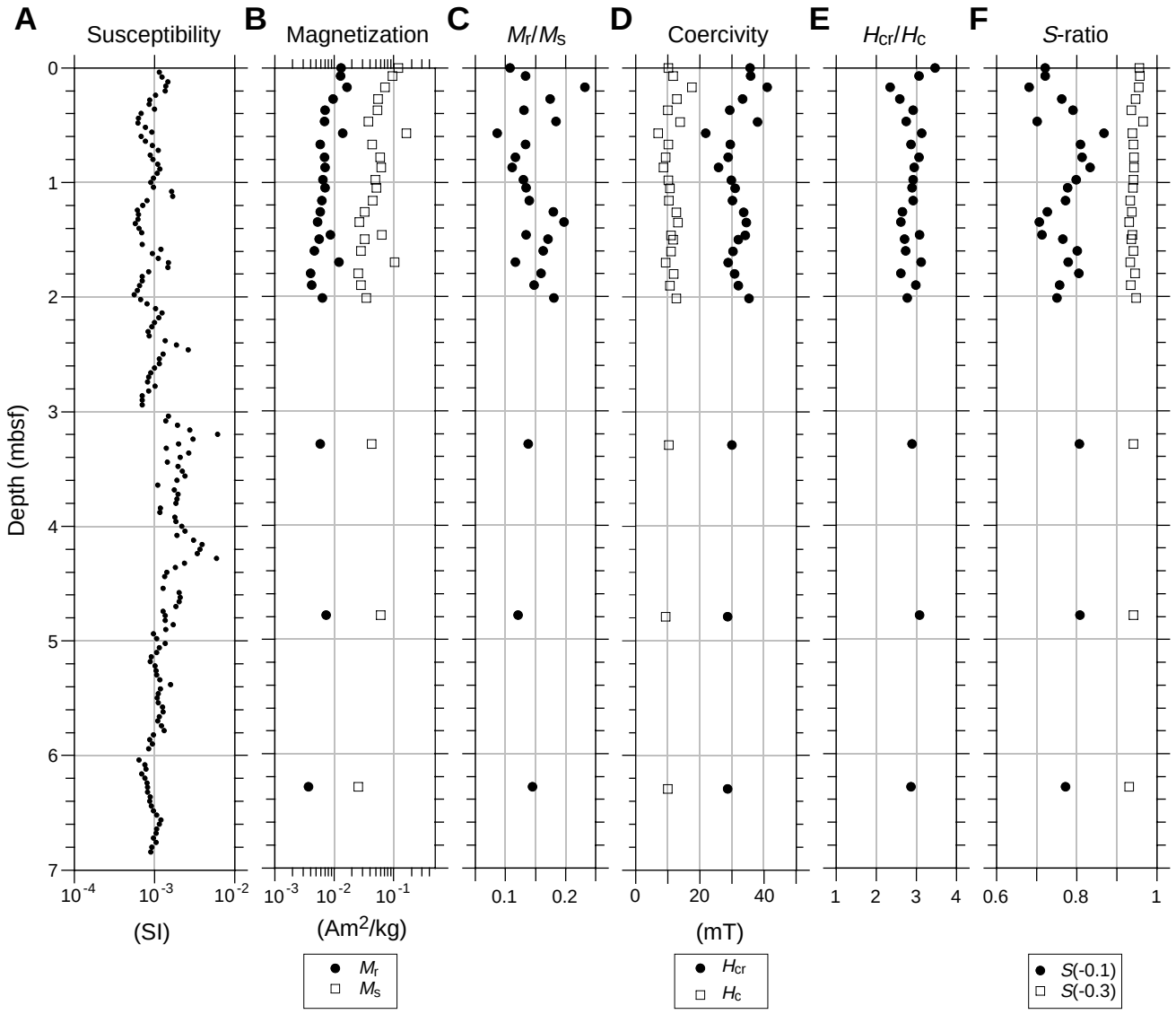

Figure F5. Bilogarithmic plots of hysteresis ratios for Sites 1109, 1115, and 1110. Arrows indicate samples in the oxidized zone at Sites 1109 and 1115. SD-MD = the mixture of single domain and multidomain magnetite (Parry, 1982).

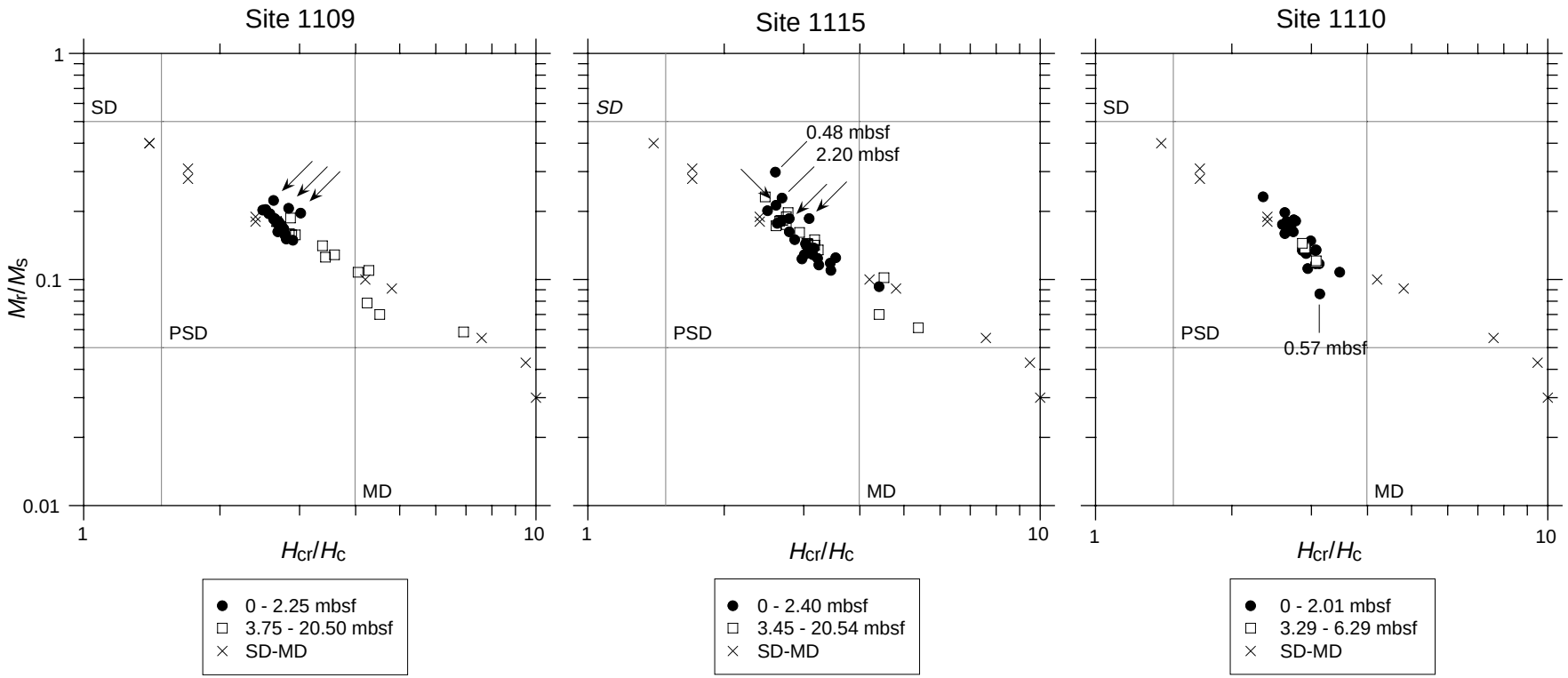

Figure F6. A.–F. Examples of hysteresis loops before and after slope correction.

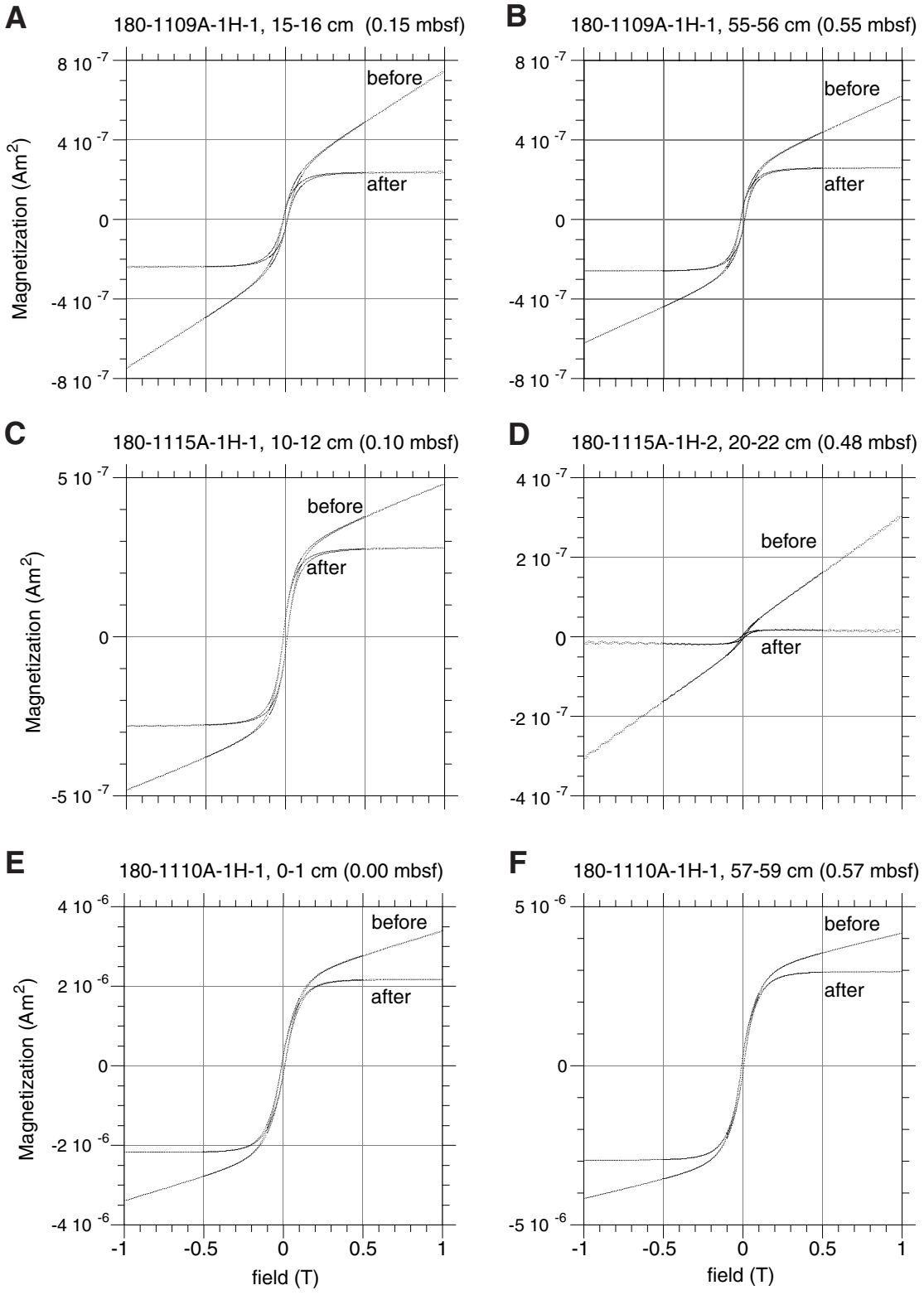

Table T1. Results of hysteresis measurements on a nickel standard sample.

	H_c (mT)	M_r (nAm^2)	M_s (nAm^2)	M_r/M_s	High-field slope (nAm^2/T)
Nickel standard sample					
Mean	4.281	246.4	439.1	0.5611	–82.82
Standard deviation	0.029	3.2	4.2	0.0067	6.23
Nickel standard sample lapped by aluminum foil					
Mean	4.286	245.2	437.9	0.5601	–50.22
Standard deviation	0.044	8.2	13.7	0.0065	17.07

Notes: H_c = coercivity, M_r = saturation remanent magnetization, M_s = saturation magnetization, high-field slope = high-field slope value between 0.7 and 1.0 T. Hysteresis measurements were performed 10 times on a nickel standard sample and the same sample lapped by a piece of aluminum foil (~8 mm^2). The aluminum piece was replaced by a new one before each measurement. The mass of the aluminum pieces ranged from 2.53 to 3.41 mg, and the mean was 3.01 ± 0.23 mg. The M_s value of the nickel standard sample = 440 nAm^2 and was used for the system calibration of the magnetometer at the first measurement of the standard sample.

Table T2. Rock magnetic parameters, Sites 1109, 1110, and 1115. (See table notes. Continued on next page.)

Core, section, interval (cm)	Depth (mbsf)	Magnetization parameters			Coercivity parameters			S-ratios	
		M_s (Am^2/kg)	M_r (Am^2/kg)	M_r/M_s	H_{cr} (mT)	H_c (mT)	H_{cr}/H_c	S (–0.1)	S (–0.3)
180-1109A-									
1H-1, 0–1	0.00	3.22E–03	1.56E–02	2.07E–01	41.16	14.50	2.84	0.626	0.944
1H-1, 5–6	0.05	4.97E–03	2.22E–02	2.24E–01	42.02	15.99	2.63	0.604	0.940
1H-1, 15–16	0.15	3.09E–03	1.57E–02	1.97E–01	42.00	13.92	3.02	0.605	0.955
1H-1, 25–26	0.25	2.37E–03	1.22E–02	1.95E–01	31.71	12.32	2.57	0.808	0.942
1H-1, 35–36	0.35	3.86E–03	1.89E–02	2.04E–01	31.39	12.43	2.53	0.797	0.942
1H-1, 45–46	0.45	3.20E–03	1.64E–02	1.95E–01	31.58	12.24	2.58	0.792	0.937
1H-1, 55–56	0.55	3.10E–03	1.52E–02	2.03E–01	32.10	12.88	2.49	0.790	0.949
1H-1, 65–66	0.65	3.64E–03	1.96E–02	1.86E–01	31.17	11.78	2.65	0.802	0.949
1H-1, 75–76	0.75	4.57E–03	2.66E–02	1.72E–01	30.11	10.97	2.74	0.809	0.946
1H-1, 85–86	0.85	3.10E–03	1.69E–02	1.83E–01	30.51	11.49	2.66	0.834	0.960
1H-1, 95–96	0.95	4.07E–03	2.20E–02	1.85E–01	31.47	11.97	2.63	0.811	0.944
1H-1, 105–106	1.05	4.00E–03	2.33E–02	1.72E–01	29.93	10.92	2.74	0.813	0.946
1H-1, 115–116	1.15	5.21E–03	2.90E–02	1.79E–01	30.96	11.43	2.71	0.794	0.939
1H-1, 125–126	1.25	4.04E–03	2.28E–02	1.77E–01	30.02	11.22	2.68	0.812	0.947
1H-1, 135–136	1.35	4.90E–03	3.24E–02	1.51E–01	28.76	10.25	2.81	0.813	0.938
1H-1, 145–146	1.45	4.55E–03	2.90E–02	1.57E–01	29.55	10.58	2.79	0.808	0.947
1H-2, 5–6	1.55	5.81E–03	3.46E–02	1.68E–01	29.96	10.81	2.77	0.811	0.941
1H-2, 15–16	1.65	6.19E–03	3.88E–02	1.60E–01	29.62	10.61	2.79	0.817	0.942
1H-2, 35–36	1.85	5.57E–03	3.74E–02	1.49E–01	29.78	10.28	2.90	0.809	0.942
1H-2, 45–46	1.95	5.11E–03	3.26E–02	1.57E–01	29.51	10.55	2.80	0.818	0.947
1H-2, 55–56	2.05	4.76E–03	2.86E–02	1.66E–01	29.22	10.69	2.73	0.814	0.942
1H-2, 65–66	2.15	4.64E–03	2.85E–02	1.63E–01	29.09	10.82	2.69	0.837	0.951
1H-2, 75–76	2.25	2.90E–03	1.67E–02	1.74E–01	30.97	11.31	2.74	0.814	0.942
1H-3, 75–76	3.75	3.30E–03	1.95E–02	1.69E–01	31.36	11.47	2.73	0.809	0.951
1H-4, 75–76	5.25	3.25E–03	1.81E–02	1.80E–01	31.75	11.91	2.67	0.839	0.943
1H-5, 75–76	6.75	2.96E–03	1.58E–02	1.87E–01	35.36	12.33	2.87	0.710	0.931
1H-6, 75–76	8.25	2.76E–03	2.50E–02	1.10E–01	32.04	7.50	4.27	0.699	0.907
1H-7, 55–56	9.55	4.82E–03	3.42E–02	1.41E–01	31.76	9.43	3.37	0.788	0.935
2H-2, 67–70	9.57	5.60E–03	9.51E–02	5.88E–02	29.30	4.24	6.92	0.710	0.883
2H-3, 111–115	11.52	4.55E–03	3.53E–02	1.29E–01	30.75	8.56	3.59	0.764	0.927
2H-4, 75–78	12.65	3.11E–03	2.47E–02	1.26E–01	29.59	8.64	3.43	0.737	0.913
2H-5, 74–77	14.14	3.34E–03	2.10E–02	1.59E–01	29.71	10.41	2.85	0.821	0.937
2H-6, 73–75	15.63	1.74E–03	1.61E–02	1.08E–01	29.70	7.34	4.05	0.785	0.920
2H-7, 31–34	16.71	3.06E–03	1.93E–02	1.58E–01	31.87	10.85	2.94	0.821	0.938
3H-1, 60–62	17.50	1.70E–03	2.15E–02	7.89E–02	29.11	6.86	4.24	0.790	0.915
3H-2, 60–62	19.00	5.01E–03	7.16E–02	7.00E–02	28.25	6.26	4.52	0.784	0.912
3H-3, 60–62	20.50	2.85E–03	1.80E–02	1.58E–01	30.94	10.75	2.88	0.820	0.948
180-1110A-									
1H-1, 0–1	0.00	1.30E–02	1.20E–01	1.08E–01	35.72	10.29	3.47	0.722	0.956
1H-1, 7–9	0.07	1.29E–02	9.61E–02	1.34E–01	35.87	11.68	3.07	0.721	0.957
1H-1, 17–19	0.17	1.66E–02	7.14E–02	2.32E–01	41.00	17.48	2.35	0.682	0.955
1H-1, 27–29	0.27	9.59E–03	5.48E–02	1.75E–01	33.30	12.84	2.59	0.763	0.947
1H-1, 37–39	0.37	7.07E–03	5.41E–02	1.31E–01	29.31	10.00	2.93	0.791	0.937
1H-1, 47–49	0.47	6.89E–03	3.75E–02	1.84E–01	38.11	13.84	2.75	0.702	0.965
1H-1, 57–59	0.57	1.41E–02	1.63E–01	8.64E–02	21.79	6.95	3.13	0.868	0.939
1H-1, 67–69	0.67	5.86E–03	4.37E–02	1.34E–01	29.49	10.27	2.87	0.810	0.941
1H-1, 78–80	0.78	6.96E–03	5.93E–02	1.17E–01	28.78	9.39	3.07	0.814	0.943
1H-1, 87–89	0.87	7.02E–03	6.25E–02	1.12E–01	25.80	8.73	2.95	0.833	0.943
1H-1, 98–100	0.98	6.41E–03	4.94E–02	1.30E–01	29.89	10.24	2.92	0.799	0.942
1H-1, 105–107	1.05	7.02E–03	5.18E–02	1.35E–01	30.99	10.70	2.90	0.777	0.940
1H-1, 116–118	1.16	6.19E–03	4.43E–02	1.40E–01	30.17	10.32	2.92	0.772	0.934
1H-1, 126–128	1.26	5.90E–03	3.28E–02	1.80E–01	33.64	12.70	2.65	0.727	0.938
1H-1, 135–137	1.35	5.26E–03	2.66E–02	1.98E–01	34.44	13.14	2.62	0.707	0.931
1H-1, 146–148	1.46	8.61E–03	6.36E–02	1.35E–01	34.22	11.10	3.08	0.713	0.939
1H-2, 0–2	1.50	5.62E–03	3.29E–02	1.71E–01	31.98	11.80	2.71	0.766	0.936
1H-2, 10–12	1.60	4.63E–03	2.84E–02	1.63E–01	30.40	11.09	2.74	0.802	0.942
1H-2, 20–22	1.70	1.20E–02	1.03E–01	1.17E–01	28.90	9.26	3.12	0.779	0.934
1H-2, 30–32	1.80	3.98E–03	2.51E–02	1.59E–01	30.95	11.83	2.62	0.806	0.945
1H-2, 40–42	1.90	4.21E–03	2.84E–02	1.48E–01	31.96	10.69	2.99	0.758	0.935
1H-2, 51–53	2.01	6.29E–03	3.48E–02	1.81E–01	35.37	12.75	2.77	0.750	0.949
1H-3, 29–31	3.29	5.84E–03	4.22E–02	1.38E–01	29.92	10.33	2.90	0.807	0.942
1H-4, 29–31	4.79	7.33E–03	6.07E–02	1.21E–01	28.72	9.33	3.08	0.808	0.941
1H-5, 29–31	6.29	3.66E–03	2.51E–02	1.45E–01	28.72	10.00	2.87	0.772	0.931
180-1115A-									
1H-1, 0–1	0.00	2.79E–03	1.31E–02	2.13E–01	37.64	14.41	2.61	0.663	0.937

Table T2 (continued).

Core, section, interval (cm)	Depth (mbsf)	Magnetization parameters			Coercivity parameters			*S*-ratios	
		M_s (Am^2/kg)	M_r (Am^2/kg)	M_r/M_s	H_{cr} (mT)	H_c (mT)	H_{cr}/H_c	*S* (–0.1)	*S* (–0.3)
1H-1, 10–12	0.10	2.74E–03	1.47E–02	1.86E–01	38.98	12.60	3.09	0.650	0.943
1H-1, 20–22	0.20	2.78E–03	1.49E–02	1.86E–01	37.40	13.41	2.79	0.624	0.936
1H-2, 0–2	0.28	1.58E–03	1.10E–02	1.44E–01	32.43	10.70	3.03	0.780	0.936
1H-2, 10–12	0.38	9.47E–04	4.68E–03	2.02E–01	31.57	12.62	2.50	0.803	0.960
1H-2, 20–22	0.48	2.82E–04	9.44E–04	2.99E–01	32.16	12.35	2.60	0.783	0.927
1H-2, 30–32	0.58	2.99E–03	2.42E–02	1.23E–01	28.14	9.46	2.98	0.819	0.941
1H-2, 40–42	0.68	2.51E–03	2.01E–02	1.25E–01	30.79	8.73	3.53	0.767	0.929
1H-2, 50–52	0.78	1.44E–03	1.10E–02	1.31E–01	30.49	9.85	3.09	0.771	0.924
1H-2, 60–62	0.88	2.73E–03	2.12E–02	1.29E–01	29.50	9.81	3.01	0.804	0.942
1H-2, 70–72	0.98	2.44E–03	1.97E–02	1.24E–01	30.84	9.59	3.22	0.752	0.930
1H-2, 80–82	1.08	1.79E–03	9.97E–03	1.80E–01	30.85	11.56	2.67	0.823	0.944
1H-2, 90–92	1.18	1.93E–03	1.39E–02	1.38E–01	34.93	11.04	3.16	0.715	0.933
1H-3, 0–2	1.50	1.69E–03	1.12E–02	1.50E–01	32.25	11.25	2.87	0.753	0.899
1H-3, 10–12	1.60	1.27E–03	9.04E–03	1.41E–01	30.32	9.95	3.05	0.815	0.942
1H-3, 20–22	1.70	1.84E–03	1.59E–02	1.16E–01	30.25	9.33	3.24	0.811	0.934
1H-3, 30–32	1.80	2.35E–03	1.82E–02	1.29E–01	29.87	9.52	3.14	0.822	0.941
1H-3, 40–42	1.90	1.56E–03	1.43E–02	1.10E–01	27.02	7.83	3.45	0.836	0.934
1H-3, 50–52	2.00	3.25E–03	3.49E–02	9.32E–02	31.04	7.03	4.41	0.791	0.937
1H-3, 60–62	2.10	2.96E–03	2.51E–02	1.18E–01	30.59	8.88	3.44	0.816	0.942
1H-3, 70–72	2.20	5.56E–04	2.43E–03	2.29E–01	32.59	12.11	2.69	0.788	0.930
1H-3, 80–82	2.30	1.14E–03	6.95E–03	1.63E–01	30.58	10.96	2.79	0.843	0.939
1H-3, 90–92	2.40	2.40E–03	1.35E–02	1.77E–01	32.53	12.41	2.62	0.792	0.941
1H-4, 45–47	3.45	3.00E–03	1.58E–02	1.90E–01	36.38	13.25	2.75	0.685	0.935
1H-CC, 10–12	4.30	3.62E–03	2.09E–02	1.73E–01	30.64	11.72	2.61	0.799	0.944
180-1115B-									
1H-3, 44–46	3.44	2.84E–03	2.11E–02	1.35E–01	32.91	10.19	3.23	0.755	0.943
1H-3, 129–131	4.29	2.17E–03	1.50E–02	1.45E–01	29.90	9.80	3.05	0.789	0.938
1H-3, 139–141	4.39	6.79E–03	4.54E–02	1.50E–01	34.48	10.87	3.17	0.736	0.940
1H-4, 44–46	4.94	4.33E–03	3.00E–02	1.44E–01	33.31	10.85	3.07	0.727	0.946
1H-5, 43–45	6.43	2.99E–03	4.86E–02	6.14E–02	27.28	5.06	5.39	0.823	0.915
2H-1, 39–41	7.59	4.80E–03	6.84E–02	7.01E–02	28.63	6.51	4.40	0.780	0.919
2H-2, 39–41	9.09	2.09E–03	1.19E–02	1.75E–01	34.14	12.40	2.75	0.774	0.934
2H-3, 44–46	10.59	1.41E–03	8.72E–03	1.62E–01	33.88	11.52	2.94	0.756	0.941
2H-4, 42–44	12.14	7.32E–03	7.19E–02	1.02E–01	36.57	8.11	4.51	0.673	0.919
2H-5, 45–47	13.62	4.56E–03	3.21E–02	1.42E–01	33.32	10.52	3.17	0.737	0.934
2H-6, 44–46	15.15	3.02E–03	1.67E–02	1.81E–01	29.80	11.21	2.66	0.860	0.953
2H-7, 89–91	16.64	2.34E–03	1.28E–02	1.83E–01	31.45	11.66	2.70	0.792	0.946
3H-1, 89–91	17.59	3.77E–03	1.90E–02	1.98E–01	37.47	13.54	2.77	0.649	0.916
3H-2, 89–91	19.09	2.53E–03	1.09E–02	2.32E–01	34.02	13.78	2.47	0.792	0.940
3H-3, 84–86	20.54	1.52E–03	8.32E–03	1.83E–01	30.18	11.29	2.67	0.841	0.956

Notes: M_r = saturation remanent magnetization, H_c = coercivity, H_{cr} = coercivity of remanence. *S* (–0.1) and *S* (–0.3) = ratios of isothermal remanence at back fields of 0.1 and 0.3 T to M_r, respectively.